International Journal of Computing and Digital Systems
ISSN (2210-142X)
Int. J. Com. Dig. Sys. 6, No.6 (Nov-2017)
http://dx.doi.org/10.12785/ijcds/060604

Performance Evaluation of a Tape-Wound Core Transformer using Meta-Model Based Scaling Laws

Ahmed Tahir[1], Abdelsalam Elhaffar[2], Scott Sudhoff[3] and Steve Pekarek[3]

[1]*Electrical and Electronics Engineering Department, University of Benghazi, Benghazi, Libya*
[2]*Electrical and Computer Engineering Department, Sultan Qaboos University, Muscat, Oman*
[3]*School of Electrical and Computer Engineering, Purdue University, West Lafayette, IN, USA*

Received 29 Jun. 2017, Revised 23 Sep. 2017, Accepted 2 Oct. 2017, Published 1 Nov. 2017

Abstract: Due to their several advantages, tape-wound core transformers are used in various power electronic systems. To obtain the optimal designs of the transformer using multi-objective optimization techniques, the effect of its performance on the whole system should be accounted for without computational liability. This may be achieved by deriving a meta-model based on scaling laws which relate the transformer performance equations to general quantities such as rated power, frequency and current density. A per-unit T-equivalent circuit and magnetic equivalent circuit model are used to obtain the transformer scaled model. By using genetic-algorithms based multi-objective optimization and curve fitting techniques, the transformer meta-model is derived. The derived meta-model is used to study the effect of varying frequency and rated power on the transformer performance.

Keywords: MEC model; Operating point analysis; Scaling laws; Tape-wound core transformer; T-equivalent circuit; Meta-model

1. INTRODUCTION

Tape-wound transformers are used in numerous applications, including power distribution, galvanic isolation, amplifiers, and dc-dc converters [1]-[4]. An advantage of tape-wound transformers is that there is no airgap in the core. In contrast, in stacked lamination designs, cores are typically assembled by bonding U or I segments together, which creates an effective airgap, which increases the Magnetomotive force (MMF) necessary to obtain a desired flux level in the core.

In order to analyze and design a tape-wound transformer, a model of the transformer is required. This may be achieved by using finite element analysis [5]-[6] or analytical techniques [7]-[12]. Since finite element analysis is computationally very expensive, analytical model is considered herein. The T-equivalent circuit in conjunction with the magnetic equivalent circuit (MEC) model [8]-[12] is considered in the work herein. The transformer operating point analysis may be conducted by establishing coupling between the MEC and a T-equivalent circuit which includes a core resistance to model core loss, to iteratively establish transformer performance from specified primary voltage and load impedance. To do so, the approach proposed in [9] is applied.

Specifically, the MEC model is used to establish leakage inductances and an initial guess of the magnetizing inductance. From these values, the T-equivalent circuit is used to predict magnetizing and secondary voltages and currents, as well as the primary current. These values are then used to update the magnetizing inductance. In addition, the winding currents are input to the MEC model to calculate core flux densities, which are used to update the core resistance. The final iteration is then used to obtain transformer performance, which includes voltage regulation, in-rush current, core loss, and winding loss.

After performing the operating point analysis, Multi-objective optimization techniques, such as particle swarm [11], or genetic algorithms [12]-[15], may be used to obtain optimal designs of the transformer. Genetic algorithms (GAs) is used herein to perform a multi objective optimization to obtain the optimal designs based on trade-off between transformer mass and total loss [12]-[15]. In this optimization process, the winding and core geometries and material properties are considered as free or arbitrary parameters. In order to obtain practical designs, constraints include limits on in-rush current, physical dimensions of the transformer, mass, voltage regulation, current density, bending radius, winding height, no-load voltage, and primary current amplitude are

E-mail address: ahmed.taher@uob.edu.ly, a.elhaffar@squ.edu.com, sudhoff@purdue.edu, spekarek@purdue.edu

imposed. The total mass and total loss correspond to each set of free parameters are evaluated. The process is repeated to obtain a Pareto-optimal front that constitutes the trade-off between the transformer mass and loss.

However, when the transformer is a component in a multiple component system, it is not accurate to optimize each component separately since the performance of one component such as temperature affects the performance of another component in the system [13]. On the other hand, the optimization based design of the system may not converge to the desired solution when all components are considered as a single optimization problem.

To resolve this issue, scaling laws are used to derive a meta-model for the transformer [13]. In the work herein, the meta-model is derived for the tape-wound transformer. Using the normalized MEC model and the multi-objective optimization approach, pareto-optimal front between normalized mass and normalized loss is obtained. Then the curve fitting techniques are used to obtain the meta-model which represent the optimum designs as a function of the transformer rated power, operating frequency, and current density.

The contribution of this work to the one discussed in [13] is that:
(*i*) Core loss is included
(*ii*) Voltage regulation is included
(*iii*) The meta-model is a function of frequency
(*iv*) The derived meta-model is used to conduct the transformer performance evaluation.

2. TAPE-WOUND TRANSFORMER GEOMETRY

Prior to deriving the scaling laws, it is useful to define the dimensions of the transformer considered as well as the T-equivalent circuit that is used in concert with the MEC. A cross-sectional view taken from the front of a core-type tape wound transformer is shown in Fig. 1. The grey region is the core, the lighter orange region is the α-winding and the darker orange region is the β-winding. The variables α and β are used to denote secondary and primary windings, respectively. As depicted in Fig. 1 the core corners are curved and not rectangular since the core considered herein is tape wound. The advantage of curvature is the reduction of saturation at the corners which may improve the transformer performance. The bending of a coil is accomplished at a certain radius which is proportional to the radius of the coil conductors as illustrated by the top cross-sectional view shown in Fig. 2. Thus, parallel conductors are generally used to reduce the bending radius.

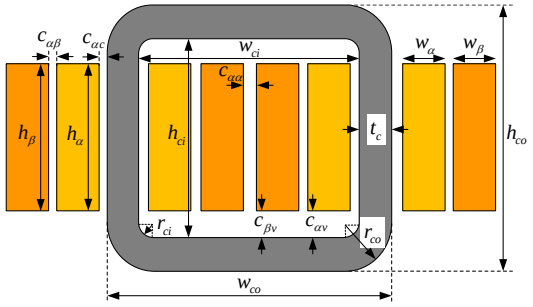

Figure 1. Tape-Wound Transformer Front Cross-Section View

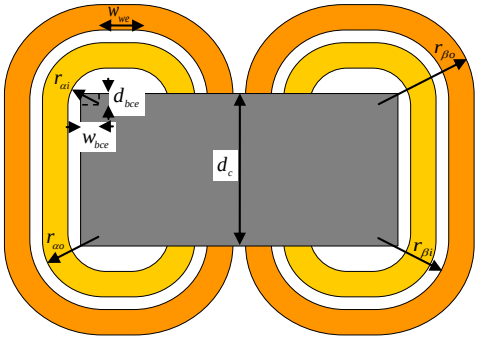

Figure 2. Tape-Wound Transformer Top View

3. SCALING LAWS AND NORMALIZATION BASE

The objective of this section is to set the stage for the normalization process by defining the normalization base. The goal is to scale all quantities tied to ratings (i.e. dimensions) and not those that are rating independent (i.e. flux density and field intensity) [13].

Since the transformer key equations and design constraints can be expressed in terms of current density, the current density is considered as a good candidate to be a parameter in the scaling laws (in addition to power and frequency). Another advantage of selecting the current density as a parameter is that it is a general quantity. In other words, a particular value of the current density may correspond to a wide range of transformer sizes, power ratings, and voltage levels.

A. *Geometrical Quantities*

The linear dimensions are scaled as [13]

$$\hat{x} = x / D \tag{1}$$

In (1), the notation '^' denotes the scaled quantity and D is the normalization base. The area and volume are scaled accordingly using [13]

$$\hat{a} = a / D^2 \tag{2}$$

$$\hat{U} = U / D^3 \tag{3}$$

Since mass is obtained by multiplying the volume by the mass density which depend only on the material type then from (3)

$$\hat{M} = M / D^3 \tag{4}$$

B. Electrical Quantities

As mentioned earlier, it is not desired to scale the flux density when deriving the meta-model. To achieve that, the current must be scaled as [13]

$$\hat{i} = i / D \tag{5}$$

The current density of winding j is defined as

$$J_j = \frac{N_{jcl} i_{jc}}{k_{jpf} A_{jcl}} \tag{6}$$

where N_{jcl}, i_{jc}, k_{jpf}, and A_{jcl} are the number of turns, current, packing factor, and cross-sectional area of coil j respectively.

Applying (2) and (5) to (6), the scaled current density is [13]

$$\hat{J} = JD \tag{7}$$

The flux linkage associated with j-winding is expressed as

$$\lambda_j = N_j \int_{S_j} B \cdot ds \tag{8}$$

where S_j is the surface.

Since the flux density is not scaled [13], then from (2), the scaled flux linkage can be expressed

$$\hat{\lambda} = \lambda / D^2 \tag{9}$$

The j- winding instantaneous voltage is calculated using

$$v_j = \frac{l_j N_j}{\sigma a_j} i_j + \frac{d\lambda_j}{dt} \tag{10}$$

where l_j and a_j are the winding j wire length and area respectively, i_j is winding j instantaneous current and σ is the winding conductor material conductivity.

If time is scaled as [9]

$$\hat{t} = t / D^2 \tag{11}$$

then from (1), (2), (5), and (9), the voltage can be expressed in terms of scaled quantities as [13]

$$v_j = \frac{\hat{l}_j N_j}{\sigma \hat{a}_j} \hat{i}_j + \frac{d\hat{\lambda}_j}{\hat{dt}} \tag{12}$$

From which one can observe that voltage is not scaled.

The frequency is the reciprocal of time and therefore, from (11) the frequency is scaled as

$$\hat{f} = fD^2 \tag{13}$$

The scaled rated power is defined as [9]

$$\hat{S}_r = S_r / D \tag{14}$$

C. Normalization Base Selection

The selection of the normalization base is a very crucial step. Since transformers are typically defined in terms of the rated power, the base of normalization is selected to be the rated power; thus,

$$D = S_r \tag{15}$$

D. Nominal Design Performance

Before starting the scaled design process, it is useful to explain how one can apply the equations derived thus far to a specific design. If the voltage of winding j and transformer rated power are defined, then the winding j rated current is calculated using

$$I_j = \frac{S_r}{V_j} \tag{16}$$

If the winding j current density is defined and the winding dimensions are known, then the number of turns for the corresponding winding is calculated using (6). After calculating the current density, the transformer performance equations can be evaluated.

4. TAPE-WOUND TRANSFOREMR SCALED MODEL

Now, the scaling laws derived in the previous section are applied to the tape-wound transformer. Prior to doing so, it is convenient to consider the T-equivalent circuit shown in Fig. 3 [9].

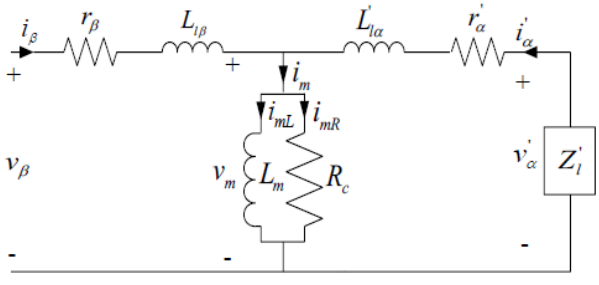

Figure 3. Transformer T-equivalent Circuit

The development of a magnetic equivalent circuit (MEC) model enables efficient magnetic analysis and design. As concluded in [10], the MEC model shown in Fig.4 can be used to represent the transformer magnetic equivalent circuit within reasonable accuracy. The MEC model shown in Fig. 4 is used in conjunction with the T-equivalent circuit to perform the transformer operating point analysis and to evaluate the transformer performance.

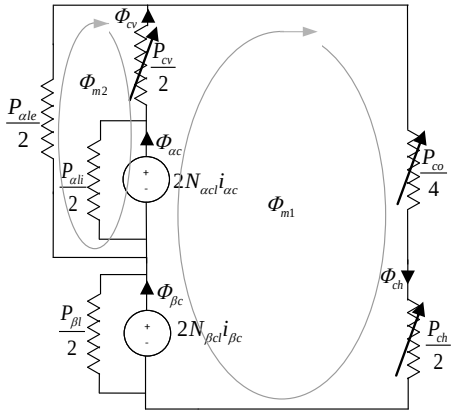

Figure 4. Reduced Magnetic Equivalent Circuit

The scaled T-equivalent circuit parameters need to be independent of number of turns. To achieve that, the per unit value $f^{(p.u)}$ which correspond to an actual quantity f is defined as

$$f^{(p.u)} = \frac{f}{f_{base}} \tag{17}$$

Using the per-unit definition and the scaling laws derived in the previous section along with the T-equivalent circuit model shown in Fig. 3 and the MEC model shown in Fig. 4, the scaled parameters of the T-equivalent circuit may be obtained. The scaled per-unit value of the linear magnetizing inductance is expressed as

$$\hat{L}_{m0}^{(p.u)} = \hat{Y}_b^{pst} \frac{\hat{\Phi}_{ac}\Big|_{\hat{J}_\beta=\hat{J}_{\beta,t},\hat{J}_\alpha=0}}{N_{\beta cs}N_{\beta cp}\hat{J}_{\beta,t}k_{\beta pf}\hat{A}_{\beta cl}} \tag{18}$$

The scaled per-unit values of the leakage inductances of the α-winding and β-winding are respectively expressed as

$$\hat{L}_{l\alpha}^{(p.u)} = \hat{Y}_b^{pst}\left(\frac{\hat{\Phi}_{ac}\Big|_{\hat{J}_\beta=0,\hat{J}_\alpha=\hat{J}_{\alpha,t}}}{N_{acs}N_{acp}\hat{J}_{a,t}k_{apf}\hat{A}_{acl}} - \frac{\hat{\Phi}_{ac}\Big|_{\hat{J}_\beta=\hat{J}_{\beta,t},\hat{J}_\alpha=0}}{N_{\beta cs}N_{\beta cp}\hat{J}_{\beta,t}k_{\beta pf}\hat{A}_{\beta cl}}\right) \tag{19}$$

$$\hat{L}_{l\beta}^{(p.u)} = \hat{Y}_b^{pst}\left(\frac{\hat{\Phi}_{\beta c}\Big|_{\hat{J}_\beta=\hat{J}_{\beta,t},\hat{J}_\alpha=0} - \hat{\Phi}_{ac}\Big|_{\hat{J}_\beta=\hat{J}_{\beta,t},\hat{J}_\alpha=0}}{N_{\beta cs}N_{\beta cp}\hat{J}_{\beta,t}k_{\beta pf}\hat{A}_{\beta cl}}\right) \tag{20}$$

The winding resistances are obtained using

$$\hat{r}_\alpha^{(p.u)} = \hat{Y}_b^{pst}\frac{\hat{U}_{\alpha cl}}{k_{\alpha pf}\hat{A}_{\alpha cl}^2\sigma_{\alpha c}N_{\alpha cs}N_{\alpha cp}} \tag{21}$$

$$\hat{r}_\beta^{(p.u)} = \hat{Y}_b^{pst}\frac{\hat{U}_{\beta cl}}{k_{\beta pf}\hat{A}_{\beta cl}^2\sigma_{\beta c}N_{\beta cs}N_{\beta cp}} \tag{22}$$

where $\hat{Y}_b^{pst}$ is the base conductance per square turn which is defined as

$$\hat{Y}_b^{pst} = \frac{\left(k_{\beta pf}\hat{A}_{\beta cl}\hat{J}_{base}N_{\beta cs}N_{\beta cp}\right)^2}{\hat{S}_{base}} \tag{23}$$

It is noted from the latest equations that the scaled per-unit quantities of the T-equivalent circuit model are not functions of the number of turns. In the next section, the scaled per-unit T-equivalent circuit model will be used in conjunction with the MEC model to conduct the operating point analysis.

5. OPERATING POINT ANALYSIS

The operating point analysis is conducted using a numerical method [9]. As discussed in the previous section, the T-equivalent circuit and the MEC are expressed in terms of the p.u. quantities instead of the actual quantities. It is assumed that the analysis is performed under normal loading conditions with the assumption that the input voltage $\hat{\hat{V}}_\beta$ and the referred load impedance $\hat{Z}_l^{'}$ are constant.

The steps of the numerical method are as follows:

A. Step 1 – Magnetizing Current Density as a Function of Magnetizing Flux

Since it is not desired to specify currents and number of turns, the magnetizing curve is constructed as a relationship between the magnetizing current density and the magnetizing flux. To obtain this relationship using the MEC, the β–winding current density is set to zero and test current densities between zero and multiple of the nominal are applied to the α–winding. The magnetizing flux corresponding to a test current density $\hat{J}_m$ is calculated as

$$\hat{\Phi}_m = \hat{\Phi}_\beta\Big|_{\hat{J}_\beta=0,\,\hat{J}_\alpha=\hat{J}_m} \tag{24}$$

From this data, the current density is generated as

$$\hat{J}_{ml} = F_{Jm}\left(\hat{\Phi}_m\right) \tag{25}$$

B. Step 2 – Initialization

The p.u. value of the core resistance and the magnetizing inductance are initialized to

$$\hat{R}_c^{1(p.u)} = \infty \tag{26}$$

$$\hat{L}_m^{1(p.u)} = \hat{L}_{m0}^{(p.u)} \tag{27}$$

Also from (26) the component of the p.u. magnetizing current that flows in the core resistance is initialized to

$$\hat{i}_{mR}^{1(p.u)} = 0 \tag{28}$$

C. Step 3 – *Solving the p.u. T-equivalent Circuit*

In order to solve the T-equivalent circuit, the p.u. values obtained in the previous section are used. From the T-equivalent circuit depicted in Fig.3, the per-unit impedance at the magnetizing branch is calculated as:

$$\hat{Z}_m^{k(p.u)} = \frac{j\omega_e \hat{L}_m^{k(p.u)} \hat{R}_c^{k(p.u)}}{\hat{R}_c^{k(p.u)} + j\omega_e \hat{L}_m^{k(p.u)}} \tag{29}$$

The per unit values of the α-winding branch impedance and the referred β-winding branch impedance are defined as

$$\hat{Z}_\beta^{(p.u)} = \hat{r}_\beta^{(p.u)} + j\omega_e \hat{L}_{l\beta}^{(p.u)} \tag{30}$$

$$\hat{Z}_\alpha^{(p.u)} = \hat{r}_\alpha^{(p.u)} + j\omega_e \hat{L}_{l\alpha}^{(p.u)} \tag{31}$$

The series combination of $\hat{Z}_\alpha^{(p.u)}$ and $\hat{Z}_l^{(p.u)}$ is expressed as

$$\hat{Z}_{\alpha l}^{(p.u)} = \hat{Z}_\alpha^{(p.u)} + \hat{Z}_l^{(p.u)} \tag{32}$$

And finally, the parallel combination of $\hat{Z}_m^{k(p.u)}$ and $\hat{Z}_{\alpha l}^{(p.u)}$ is expressed as

$$\hat{Z}_{m\alpha l}^{k(p.u)} = \frac{\hat{Z}_m^{k(p.u)} \hat{Z}_{\alpha l}^{(p.u)}}{\hat{Z}_m^{k(p.u)} + \hat{Z}_{\alpha l}^{(p.u)}} \tag{33}$$

Using the impedance expressions derived in (29)-(33), the p.u magnetizing voltage and the voltage and current at the load side are calculated

$$\hat{\tilde{V}}_m^{k(p.u)} = \frac{\hat{Z}_{m\alpha l}^{k(p.u)}}{\hat{Z}_{m\alpha l}^{k(p.u)} + \hat{Z}_\beta^{(p.u)}} \hat{\tilde{V}}_\beta^{k(p.u)} \tag{34}$$

$$\hat{\tilde{V}}_\alpha^{k(p.u)} = \frac{\hat{Z}_l^{(p.u)}}{\hat{Z}_l^{(p.u)} + \hat{Z}_\alpha^{(p.u)}} \hat{\tilde{V}}_m^{k(p.u)} \tag{35}$$

$$\hat{\tilde{I}}_\alpha^{k(p.u)} = \frac{\hat{\tilde{V}}_\alpha^{k(p.u)}}{\hat{Z}_l^{(p.u)}} \tag{36}$$

It is noted form (6), (7) and (17) that the p.u current and current density are equal, thus

$$\hat{J}_\alpha^{k(p.u)} = \hat{\tilde{I}}_\alpha^{k(p.u)} \hat{J}_{base} \tag{37}$$

D. Step 4 – Magnetizing Current Density

The p.u. magnetizing voltage is assumed to be

$$\hat{v}_m^{k(p.u)} = \sqrt{2}\left|\hat{\tilde{V}}_m^{k(p.u)}\right| \sin\left(\hat{\omega}_e \hat{t} + \phi_{vm}^k\right) \tag{38}$$

The p.u magnetizing flux linkage obtained from the magnetizing voltage using Faraday's law as

$$\hat{\lambda}_m^{k(p.u)} = \frac{\sqrt{2}\left|\hat{\tilde{V}}_m^{k(p.u)}\right|}{\hat{\omega}_e} \cos\left(\hat{\omega}_e \hat{t} + \phi_{vm}^k\right) \tag{39}$$

The relationship between the p.u. flux and flux linkage is considered

$$\hat{\Phi}_m^{(p.u)} = \frac{\hat{\lambda}_m^{(p.u)}}{N_\beta} \tag{40}$$

From the definition of p.u. inductances, it can be noted that the base flux linkage is equal to the base voltage

$$\hat{\lambda}_{base} = \hat{V}_{base} \tag{41}$$

Using (6), (7), (17), (40) and (41), the actual value of the magnetizing flux can be expressed as

$$\hat{\Phi}_m^k = \frac{\hat{\lambda}_m^{k(p.u)} \hat{S}_{base}}{N_{\beta cs} N_{\beta cp} k_{\beta pf} \hat{J}_{base} \hat{A}_{\beta cl}} \tag{42}$$

Substituting the value of the magnetizing flux obtained using (42) into (25) yields the corresponding magnetizing current density then the p.u. magnetizing current is calculated as,

$$\hat{i}_{mL}^{k(p.u)}\left(\hat{t}\right) = \frac{\hat{J}_{mL}^k\left(\hat{t}\right)}{\hat{J}_{base}} \tag{43}$$

The total p.u. magnetizing current is then calculated as

$$\hat{i}_m^{k(p.u)}\left(\hat{t}\right) = \hat{i}_{mL}^{k(p.u)}\left(\hat{t}\right) + \hat{i}_{mR}^{k(p.u)}\left(\hat{t}\right) \tag{44}$$

E. Step 5 – Updating Magnetizing Branch Parameters

In this step, the p.u. magnetizing inductance and the core resistance for the following iteration are calculated. First the β-winding current is calculated

$$\hat{i}_{\beta}^{k(p.u)}\left(\hat{t}\right)=\hat{i}_{m}^{k(p.u)}\left(\hat{t}\right)-\hat{i}_{\alpha}^{k(p.u)}\left(\hat{t}\right) \tag{45}$$

The current density of the β-winding is then calculated as

$$\hat{\vec{J}}_{\beta}=\hat{\vec{I}}_{\beta}^{k(p.u)}\hat{J}_{base} \tag{46}$$

The mmf of the j-winding is defined as

$$\hat{mmf}_{j}^{k}=2\hat{J}_{j}^{k}k_{jpf}\hat{A}_{jcl} \tag{47}$$

Using the MEC depicted in Fig. 3 with the winding mmfs defined in (47), the flux density in the core tube is obtained. Then the MSE is used to compute the core loss $\hat{P}_{cl}^{k}$, [9]

Using (17), the per unit core loss is calculated as

$$\hat{P}_{cl}^{k(p.u)}=\frac{\hat{P}_{cl}^{k}}{\hat{P}_{base}} \tag{48}$$

Next, the p.u. core resistance is updated

$$\hat{R}_{c}^{k+1(p.u)}=\frac{\left(\hat{V}_{m}^{k(p.u)}\right)^{2}}{\hat{P}_{cl}^{k(p.u)}} \tag{49}$$

The p.u. current in the core resistance for the next iteration is thus computed as

$$i_{mR}^{k+1(p.u)}=\frac{\hat{v}_{m}^{k(p.u)}}{\hat{R}_{c}^{k+1(p.u)}} \tag{50}$$

Next, the Fourier series is used to obtain the fundamental component of the p.u. current through the magnetizing inductance. To do so, Fourier series coefficient are expressed as

$$\hat{a}_{mL1}^{k}=\frac{4}{\hat{T}}\int_{0}^{\hat{T}/2}i_{mL}^{k(p.u)}\left(\hat{t}\right)\cos\left(\hat{\omega}_{e}\hat{t}\right)d\hat{t} \tag{51}$$

$$\hat{b}_{mL1}^{k}=\frac{4}{\hat{T}}\int_{0}^{\hat{T}/2}i_{mL}^{k(p.u)}\left(\hat{t}\right)\sin\left(\hat{\omega}_{e}\hat{t}\right)d\hat{t} \tag{52}$$

The p.u. rms value of the magnetizing current through the magnetizing inductance is computed as

$$\hat{I}_{mL}^{k(p.u)}=\frac{1}{\sqrt{2}}\sqrt{\left(\hat{a}_{mL1}^{k}\right)^{2}+\left(\hat{b}_{mL1}^{k}\right)^{2}} \tag{53}$$

Subsequently, p.u. value of the magnetizing inductance for the next iteration is updated as

$$\hat{L}_{m}^{k+1(p.u)}=\frac{\hat{V}_{m}^{k(p.u)}}{\hat{\omega}_{e}\hat{I}_{mL}^{k(p.u)}} \tag{54}$$

F. Step 6 – Checking the Convergence

To check the convergence, the error metrics are defined

$$e=\max\left(\left|\frac{\hat{R}_{c}^{k+1(p.u)}-\hat{R}_{c}^{k(p.u)}}{\hat{R}_{c}^{k+1(p.u)}}\right|,\left|\frac{\hat{L}_{m}^{k+1(p.u)}-\hat{L}_{m}^{k(p.u)}}{\hat{L}_{m}^{k+1(p.u)}}\right|\right) \tag{55}$$

In (55), if the error is less than the maximum allowed error, e_{mxa}, then the algorithm proceeds to the final calculation step. Otherwise, the iterative process is repeated starting at step 3.

G. Step 7 – Final Calculations

Once convergence is obtained, the transformer total power loss is computed. The resistive power loss is calculated as

$$\hat{P}_{rl}^{(p.u)}=\hat{r}_{\beta}^{(p.u)}\left(\hat{I}_{\beta}^{(p.u)}\right)^{2}+\hat{r}_{\alpha}^{(p.u)}\left(\hat{I}_{\alpha}^{(p.u)}\right)^{2} \tag{56}$$

The p.u. total power loss is

$$\hat{P}_{l}^{(p.u)}=\hat{P}_{rl}^{(p.u)}+\hat{P}_{cl}^{(p.u)} \tag{57}$$

From (17), the actual value of the total power loss can be obtained

$$\hat{P}_{l}=\hat{P}_{l}^{(p.u)}\hat{P}_{base} \tag{58}$$

The current density in the j-winding is also calculated using

$$\hat{J}_{j}=\left|\hat{\vec{I}}_{j}^{k(p.u)}\right|\hat{J}_{base} \tag{59}$$

6. TRANSFORMER META-MODEL DERIVATION

In order to derive a meta-model which represent a wide range of transformer ratings and frequencies, a genetic algorithms based multi-objective optimization is conducted between scaled total mass $\hat{M}_{T}$ and total loss $\hat{P}_{l}$ of the transformer. To achieve that, the fitness function is defined as

$$f\left(\theta,D\right)=\begin{cases}\left[\dfrac{1}{\hat{M}_{T}}\ \dfrac{1}{\hat{P}_{l}}\right]^{T} & c=1\\ \left(c-1\right)\left[1\,1\right]^{T} & c<1\end{cases} \tag{60}$$

where the design space vector θ is defined as,

$$\theta = \left[\hat{J}_r \;\; m_c \;\; m_\beta \;\; \hat{h}_{\beta w} \;\; r_{w\beta w} \;\; m_\alpha \;\; r_{hzw} \;\; r_{wzw} \;\; r_{dw} \;\; r_{wes} \;\; r_{rci} \right] \quad (61)$$

where $\hat{h}_{\beta w}$ is the scaled height of the β-coil and the ratios r_{wjw}, $(j = \alpha, \beta)$, r_{hzw}, r_{dw}, r_{wes} and r_{rci} are defined as

$$r_{wjw} = \frac{\hat{w}_{jw}}{\hat{h}_{\beta w}} \quad (62)$$

$$r_{hzw} = \frac{\hat{h}_{zw}}{\hat{h}_{\beta w}} \quad (63)$$

$$r_{dw} = \frac{\hat{d}_w}{\hat{h}_{\beta w}} \quad (64)$$

$$r_{rci} = \frac{\hat{r}_{ci}}{\hat{h}_{\beta w}} \quad (65)$$

The design parameter encoding and range which is defined between maximum and minimum values as depicted in Table I

TABLE I. DESIGN PARAMETER ENCODING

Number	*PARAMETER*	*Minimum*	*Maximum*	*Type*
1	$\hat{J}_r$	10^8	10^{14}	Logarithmic
2	m_c	1	4	Integer
3	m_β	1	2	Integer
4	$\hat{h}_{\beta w}$	10^{-7}	10	Logarithmic
5	$r_{w\beta w}$	0.1	20	Logarithmic
6	m_α	1	2	Integer
7	r_{hzw}	0.1	20	Logarithmic
8	r_{wzw}	0.1	20	Logarithmic
9	r_{dw}	0.1	20	Logarithmic
10	r_{wes}	0.01	10	Logarithmic
11	r_{rci}	10^{-4}	10^{-3}	Logarithmic

The design specification vector D is defined in Table II

TABLE II. DESIGN SPECIFICATIONS AND FIXED PARAMETERS

Parameter	*Value*	*Parameter*	*Value*
$V_{\beta 0}^{(p.u)}$	1	N_{Jmpt}	100
$V_{\alpha nlmxa}^{(p.u)}$	1.02	N_{tpt}	50
$V_{\alpha nlmnr}^{(p.u)}$	0.98	O_{emxa}	10^{-3}
$I_{\beta nlmxa}^{(p.u)}$	0.1	O_{imxa}	10
$I_{\alpha,fl}^{(p.u)}$	1	$\hat{c}_{\alpha c\_mn}$	10^{-9}
χ_{mxa}	0.05	$\hat{c}_{\alpha\beta}$	10^{-9}
$i_{\beta imxa}^{(p.u)}$	$2\sqrt{2}$	$\hat{c}_{\beta\beta}$	10^{-9}
$\lambda_{\beta wcs}^{(p.u)}$	0.05	$\hat{c}_{\alpha v}^{*}$	10^{-9}
$\mathbf{V}_{\beta}^{(p.u)}$	[1 1]	$\hat{c}_{\beta v}^{*}$	10^{-9}
$\mathbf{Z}_{l}^{(p.u)}$	[2 1]	$k_{\alpha pf}$	0.6
$\hat{\boldsymbol{\omega}}_e$	$\hat{\omega}_e$ [1 1]	$k_{\beta pf}$	0.6
$\mathbf{W}$	[0.1 0.4 0.5]	$N_{\beta cp}$	2
$\hat{P}_{lmxa}$	0.1	$N_{\beta cs}$	1
η_{mxa}	$2\sqrt{2}/\hat{\omega}_e$	$N_{\alpha cp}$	2
$\hat{J}_{\alpha,t}$	10^{-3}	$N_{\alpha cs}$	1
$\hat{J}_{\beta,t}$	10^{-3}		

The multi-objective optimization is repeated for four different frequencies with the current density defined as a design parameter. As a result, four Pareto-optimal fronts which represent the trade-off between the scaled mass and the scaled loss are obtained. The normalized mass versus normalized current density and normalized loss versus normalized current density at each normalized frequencies are depicted in Fig. 5 and Fig. 6 respectively.

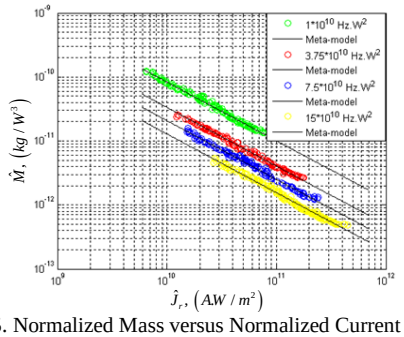

Figure 5. Normalized Mass versus Normalized Current Density

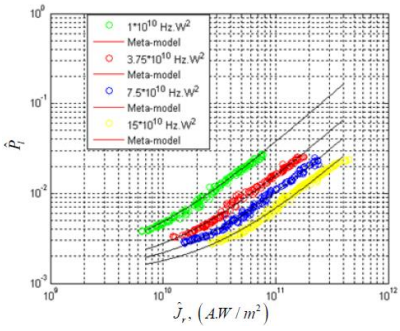

Figure 6. Normalized Loss versus Normalized Current Density

Applying curve fitting techniques to these four curves yields the transformer meta-model [13]

$$M = C_M P_r^3 \left(f P_r^2 \right)^{n_{fM}} \left(J P_r \right)^{n_{JM}} \quad (66)$$

$$P_l = C_l P_r \left(J P_r \left(f P_r^2 \right)^{n_{fl1}} + b_{Jl} \right)^{n_{Jl}} \left(f P_r^2 \right)^{n_{fl2}} \quad (67)$$

The parameters of the meta-model expressed by (66) and (67) are calculated using curve fitting techniques and listed in Table II.

TABLE III. META-MODEL PARAMETERS

Parameter	*Value*	*Parameter*	*Value*
C_M	9.218*10^5	b_{Jl}	2.907*10^4
n_{fM}	-0.9155	n_{Jl}	1.098
n_{JM}	-0.6892	n_{fl1}	-0.5345
C_l	2.993*10^{-7}	n_{fl2}	-0.1137

The parameter distribution plot is depicted in Fig. 7. As shown, each parameter tends to almost converge to a specific value except b_{Jl} which seems to have less significant contribution to the loss Meta-model equation. As shown, the parameters are normalized with zero correspond to the minimum value and one correspond to the maximum value.

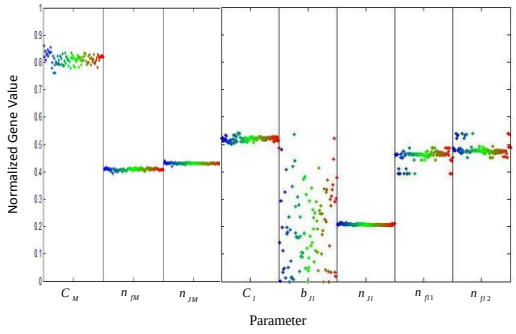

Figure 7. Distribution Plot of Meta-Model Parameters

The curves predicted by the meta-model are plotted with the original data in Fig. 5 and Fig. 6. It can be seen that the meta-model is reasonably accurate in predicting the relationship between normalized mass and loss for different values of normalized frequency and current density.

7. META-MODEL BASED PERFORMANCE EVALUATION

In the previous section, multi-objective optimization approach and curve fitting techniques were used to derive the transformer met-model. The meta-model relates the transformer total mass and power loss to the current density, frequency and rated power. In this section, the derived meta-model is used to predict the performance of a wide range of rated power, frequency, and current density.

To study the effect of the transformer rated power on the total mass and total loss, the frequency is set to 1 kHz and the current density is set to 7.6 A/mm^2 which correspond to the thermal limit for copper conductors [9]. The rated power is varied between 1 kW and 100 kW. As illustrated in Fig. 8, the total mass per kW decreases as the transformer rated power increases.

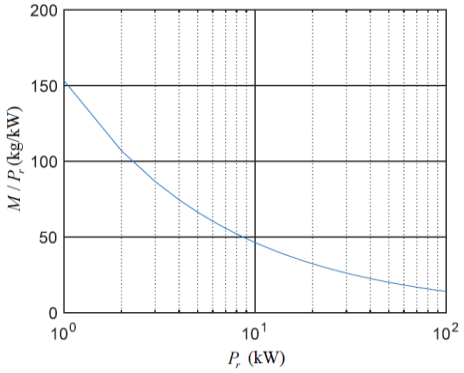

Figure 8. Total Mass per kW versus transformer rated power

The efficiency increases with increasing the transformer rated power as depicted in Fig. 9. This should be expected since the transformer performance is better for larger transformers.

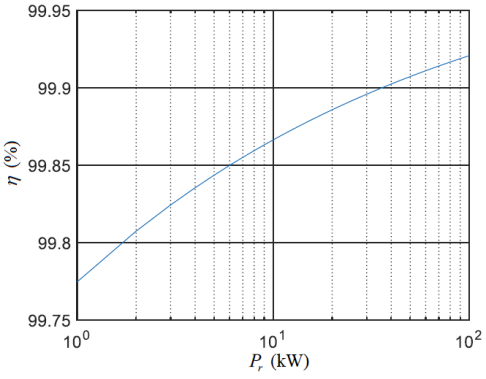

Figure 9. Efficiency versus transformer rated power

The effect of the frequency on the transformer mass is depicted in Fig. 10. By varying the frequency between 10 Hz and 1 kHz with the rated power set to 10 kW and at 7.6 A/mm^2 current density. As one may expect, the transformer total mass is inversely proportional to frequency. This explain the tendency of operating many power electronic systems at higher frequencies. Since core loss is included in the meta-model derivation, the meta-model can accurately predict the transformer performance with operating frequencies up to few kHz. The effect of the parasitic capacitances is negligible at this frequency level [10].

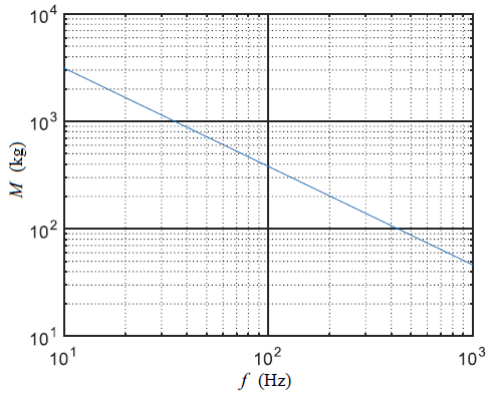

Figure 10. Total mass versus frequency

The transformer efficiency is also plotted with frequency as illustrated in Fig. 11. As shown, the efficiency improves as frequency increases which give another advantage of operating the transformer at higher frequencies.

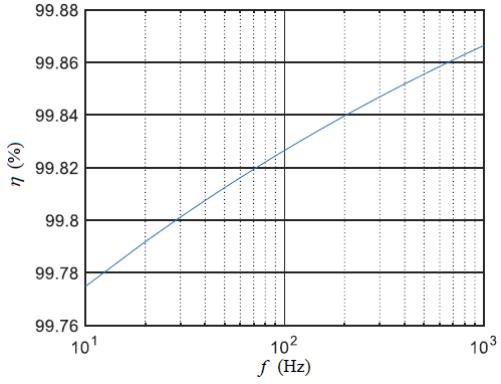

Figure 11. Efficiency versus frequency

REFERENCES

[1] Vacuumschmelze *Tape-wound cores for magnetic amplifier chokes Vitrovac 6025 Z*, Edition 1998

[2] Tsili, Marina A., Antonios G. Kladas, Pavlos S. Georgilakis, Athanasios T. Souflaris, and Dimitris G. Paparigas. "Advanced design methodology for single and dual voltage wound core power transformers based on a particular finite element model." *Electric power systems research* 76, no. 9 (2006): 729-741.

[3] Cougo, B., A. Tüysüz, J. Mühlethaler, and J. W. Kolar. "Increase of tape wound core losses due to interlamination short circuits and orthogonal flux components." In *IECON 2011-37th Annual Conference on IEEE Industrial Electronics Society*, pp. 1372-1377. IEEE, 2011.

[4] Guo, Xianqing, Danju Song, and Liqiong Long. "Study of material-saving effect of transformer with 3-D wound core." In *Electricity Distribution (CICED), 2012 China International Conference on*, pp. 1-4. IEEE, 2012.

[5] Musa, Sarhan M., and Matthew NO Sadiku. "Finite Element Approach of Unshielded Multiconductor Transmission Lines Embedded in Layered Dielectric Region for VLSI Circuits." *Int. J. Com. Dig. Sys* 1, no. 1 (2012): 25-30.

[6] Musa, Sarhan M., and Matthew NO Sadiku. "Finite element method analysis of symmetrical coupled microstrip lines." *Int. J. Com. Dig. Sys* 3, no. 3 (2014).

[7] Zadehbagheri¹, Mahmoud, Rahim Ildarabadi, and Majid Baghaei Nejad. "A Novel Method for Analysis, Modeling and Simulation of Brushless DC Motors Using MATLAB/SIMULINK." *Int. J. Com. Dig. Sys* 3, no. 3 (2014).

[8] Yilmaz, Murat, and Philip T. Krein. "Capabilities of finite element analysis and magnetic equivalent circuits for electrical machine analysis and design." In *Power Electronics Specialists Conference, 2008. PESC 2008. IEEE*, pp. 4027-4033. IEEE, 2008.

[9] Sudhoff, Scott D. *Power magnetic devices: a multi-objective design approach*. John Wiley & Sons, 2014.

[10] Taher, Ahmed, Scott Sudhoff, and Steve Pekarek. "Calculation of a tape-wound transformer leakage inductance using the MEC model." *IEEE Transactions on Energy Conversion* 30, no. 2 (2015): 541-549.

[11] Okada, Hidehiko. "Evolving fuzzy neural networks by particle swarm optimization with fuzzy genotype values." *Int. J. Com. Dig. Sys* 3, no. 3 (2014).

[12] A. Tahir, A Elhaffar, S. Sudhoff, S. Pekarek " MEC Based Scaling Laws for a Tape-Wound Transformer with Voltage Regulation and Core Loss included, " In *GCC Conference and Exhibition (GCC), 2017 9th IEEE*, pp. 1201-1206. IEEE, 2017.

[13] Sudhoff, Scott D., Grant M. Shane, and Harish Suryanarayana. "Magnetic-equivalent-circuit-based scaling laws for low-frequency magnetic devices." *IEEE Transactions on Energy Conversion* 28, no. 3 (2013): 746-755.

[14] Versele, Christophe, Olivier Deblecker, and Jacques Lobry. "Multiobjective optimal design of high frequency transformers using genetic algorithm." In *Power Electronics and Applications, 2009. EPE'09. 13th European Conference on*, pp. 1-10. IEEE, 2009.

[15] Versèle, Christophe, Olivier Deblecker, and Jacques Lobry. "Multiobjective optimal design of transformers for isolated switch mode power supplies." In *Power Electronics Electrical Drives Automation and Motion (SPEEDAM), 2010 International Symposium on*, pp. 1687-1692. IEEE, 2010.

Ahmed Tahir received the B.S. (top of his class) in electrical engineering from University of Benghazi in 2006. He received the M.S., and Ph.D. degrees in electrical engineering from Purdue University, West Lafayette, IN, in 2011 and 2014, respectively. Since the fall of 2015 he has been a teaching staff member at University of Benghazi. His current research interests include electric machines, power electronics, and renewable energy.

Abdelsalam Elhaffar received the B.sc (89) and M.Sc. (99) degrees from from University of Benghazi (formerly Garyounis University), Libya, and D. Sc. Tec. degree from Helsinki University of Technology in 2008, Finland. He has been working for the electric power company in Libya as a Protection and maintenance Engineer in the early years of his career and has been working for Helsinki University of Technology as a researcher at the Department of Electrical Engineering until 2008. He worked as an assistant professor at University of Benghazi and a consultant to several companies in the field of protections, maintenance, and troubleshooting for generator sets until 2014. Now he is with Sultan Qaboos University and on leave from UoB. His research interests include power system protection, distributed generation, smart grids, and fault location in power systems.

Scott D. Sudhoff received the B.S. (highest distinction), M.S., and Ph.D. degrees in electrical engineering from Purdue University in 1988, 1989, and 1991, respectively. From 1991-1993, he served as a consultant for P.C. Krause and Associates in aerospace power and actuation systems. From 1993 to 1997, he served as a faculty member at the University of Missouri - Rolla, and in 1997 he joined the faculty of Purdue University where he currently holds the rank of full professor. His interests include electric machinery, power electronics, marine and aerospace power systems, applied control, and evolutionary computing. Much of his current research focuses on genetic algorithms and their application to power electronic converter and electric machine design. He has published over one hundred papers in these areas, including six prize papers. He is a fellow of IEEE, served as Editor-in-Chief of *IEEE Transactions on Energy Conversion*, and currently serves as Editor-in-Chief of *IEEE Power and Energy Technology System Journal*.

Steve D. Pekarek received his PhD in Electrical Engineering from Purdue University in 1996. From 1997-2004 Dr. Pekarek was an Assistant (Associate) Professor of Electrical and Computer Engineering at the University of Missouri-Rolla (UMR). He is presently a Professor of Electrical and Computer Engineering at Purdue University and is Chair of the Energy Sources and Systems Area. He is an active member of the IEEE Power Engineering Society. He has served as the Technical Chair of the 2007 IEEE Applied Power Electronics Conference and Technical Chair of the 2013 IEEE Electric Machines and Drives Conference. He is an Editor for IEEE Transactions on Energy Conversion.